Proceedings World Geothermal Congress 2010
Bali, Indonesia, 25-29 April 2010

Effects of Pressure, Temperature, Fluid-Rock Interactions, and Phase Changes on the Physical Properties of Geothermal Reservoir Rocks: the Experimental Perspective

Harald Milsch[1], Erik Spangenberg[1], Siegfried Raab[1], Ansgar Schepers[1], Guido Blöcher[1], David Bruhn[1], Líney H. Kristinsdóttir[2], Ólafur G. Flóvenz[2] and Ernst Huenges[1]

[1]GFZ German Research Centre for Geosciences, Telegrafenberg, 14473 Potsdam, Germany

[2]Icelandic GeoSurvey (ÍSOR), Grensásvegi 9, 108 Reykjavík, Iceland

milsch@gfz-potsdam.de

Keywords: experimental rock physics, geothermal reservoir rocks, permeability, electrical conductivity, enhanced geothermal systems (EGS), North German Basin, Iceland, Italy

ABSTRACT

Within the GFZ, Section "Reservoir Technologies", there is a long-standing tradition in experimental rock physics. We maintain several high pressure (100 MPa) and high temperature (200°C) flow-through apparatuses to address questions arising in geothermal reservoir characterization, evolution and sustainability. Various research programs are conducted both site specific and process oriented. So far, the types of fluid-rock combinations explored, relate to the geothermal wells in Groß Schönebeck (Germany), Hengill and Krafla (Iceland), and Anqua and Radicondoli (Italy), respectively. With regard to particular parameters and processes related to these reservoirs we experimentally investigated:

1) The pressure dependence of rock transport properties and their interrelations (Germany), where three different models relating permeability and electrical conductivity were tested and the appropriateness of an individual model showed to be rock-type dependent.
2) The effect of dissolution-precipitation reactions on rock permeability (Germany), where in a series of long-term flow-through experiments at various chemical fluid compositions even after six months of flow no significant change in permeability in neither direction was observed.
3) The temperature dependence of electrical rock conductivity and seismic wave velocities (Iceland and Italy), where the values derived for the temperature coefficient α, were in the range 0.027-0.160 1/°C indicating the predominance of interface conduction regardless of the respective alteration stage. P-wave velocities systematically decreased with temperature and were in the range of 4.4 km/s (25°C) and 3.4 km/s (250°C).
4) The evolution of electrical rock conductivity in a fluid-rock disequilibrium (Germany and Iceland), where observed transient conductivity changes are interpreted as alterations of the fluid-rock interface properties and/or of pore fluid compositions resulting from dissolution processes.
5) The petrophysical signature of a water-steam phase transition within the pore space (Germany and Iceland), where it showed that the conduction mechanism (fluid vs. interface conduction) controls the pattern of electrical conductivity variations as steam saturation changes.

Here, we provide an outline of the technical features of our apparatuses, background information on the particular geothermal setting as well as experimental details and results of the individual projects outlined above.

1. INTRODUCTION

Effective energy production from geothermal reservoirs requires the physical properties of the host rock to be characterized as precisely as possible. This can be achieved by an appropriate combination of production and/or injection tests and borehole-logging techniques. Rock physical experiments, in addition, provide a valuable complementary method to investigate particular processes associated with mechanical and thermodynamic changes induced during operation. Not least, the results of such investigations can be included in hydro-thermo-mechanical-chemical (HTMC) simulation codes to derive statements on reservoir productivity, sustainability, and best-practice operation.

For hydrothermal settings the key parameter for reservoir productivity and indirectly its thermal evolution is the matrix permeability which in turn is affected by changes in effective stress through changes in pore space geometry (e.g. Jaeger and Cook, 1976; Blöcher et al., 2009). Furthermore, production-induced thermodynamic fluid-rock disequilibria can severely damage permeability when mineral precipitates or other fines plug the pore throats (e.g. Civan, 2000).

Electrical rock conductivity, as a second important rock transport property, is widely used in geophysical borehole-prospecting to indirectly obtain information about the formation permeability given an appropriate correlation function (e.g. Martys and Garboczi, 1992). In contrast to permeability, electrical conductivity is strongly dependent on temperature and the predominant individual conduction mechanism which can be surface or fluid dominated (Ruffet et al., 1995). Differences in the conduction mechanism yield different temperature coefficients (e.g. Revil et al., 1998) which, in addition to the pore fluid chemistry, have to be known to adequately determine the formation factor (Archie, 1942). In volcanic environments such distinctions can also assist to correctly map resistivity variations associated with different stages of alteration (Flóvenz et al., 1985).

Finally, in a thermodynamic disequilibrium the electrical rock conductivity can be altered by either changes in pore fluid chemistry (Piwinskii and Weed, 1976) and/or phase transitions (e.g. water to steam) (Roberts et al., 2001). In both cases electrical conductivity will be time dependent, in the second case it will also depend on the residual saturation provided that conduction is fluid dominated.

2. EXPERIMENTAL METHODOLOGY

For process-oriented studies in the geothermal context testing under realistic in situ pressure and temperature conditions is necessary. This also includes the selection of

an appropriate sample material and the use of the respective formation fluids as well as a continuous fluid flow through the specimen. In addition, as an evolution of the rock transport properties depends on the rates of the transformations involved, stable experimental conditions have, eventually, to be maintained over longer time periods. Finally, it is desirable not only to measure changes in the petrophysical transport properties (e.g. permeability) but one should also be able – for explanatory purposes – to complement these investigations with pore fluid sampling and an analysis of the fluid chemistry. To meet these requirements two identical devices have been set up at the GFZ being a refined derivative of an older concept described by Kulenkampff et al. (2005). Continuous flow experiments, so far, have been performed over a maximum of six months.

The apparatus consists of an internally heated oil-medium pressure vessel and a connected pore fluid system. The sample assembly is inserted vertically into the vessel. Both confining- and pore pressure are generated with piston-cylinder type syringe pumps. The apparatus allows simultaneous and continuous measurements of permeability, electrical conductivity as well as P- and S-wave velocities at maximum confining pressures, pore pressures and temperatures of 100 MPa, 50 MPa and 200 °C, respectively. Typically, the sample size is 30 mm in diameter and 40 mm in length.

The permeability of a rock is determined by a steady state method making direct use of Darcy's Law (e.g. Darcy, 1856; Scheidegger, 1974; Bear, 1988). The electrical conductivity is measured with a four-electrode arrangement. Silver rings painted onto the samples at a distance of 25 mm are used as the potential electrodes. Ultrasonic measurements are performed with piezoelectric ceramics for both compressional (P) and shear (S) waves, respectively. For the electrical conductivity- and ultrasonic measurements voltage signals are impressed with a function generator (Agilent 33220A). Typically, the voltage is an AC-sine 1.0 V peak-to-peak signal at a frequency of 13 Hz and a rectangular voltage single burst at 1.0 V and 400 kHz for conductivity- and ultrasonic measurements, respectively. For electrical conductivity the input impedance is 10 MOhms. The temperature is measured with two PT-100 sensors, one close to the top and one close to the bottom of the specimen, respectively. Generally, one notices a temperature gradient of approximately 1 - 2°C along the sample, the top side being the hotter part. The use of corrosion resistant parts throughout the pore pressure system allows investigations with highly saline formation fluids which can also be sampled under pressure for further chemical analysis. **Figures 1a, 1b, and 1c** show the general set-up of the apparatus, the individual parts of the specimen assembly, and the mounted specimen assembly, respectively.

A detailed description of the apparatus and specific measurement procedures can be found in Milsch et al. (2008a).

3. GEOTHERMAL SETTINGS ADDRESSED

3.1 North German Basin

The technical feasibility of geothermal power production from hydrothermal (sedimentary) reservoirs with normal geothermal gradients will be demonstrated by means of the geothermal research wells Groß Schönebeck (40 km north of Berlin, Germany) using a borehole doublet as shown in **Figure 2**.

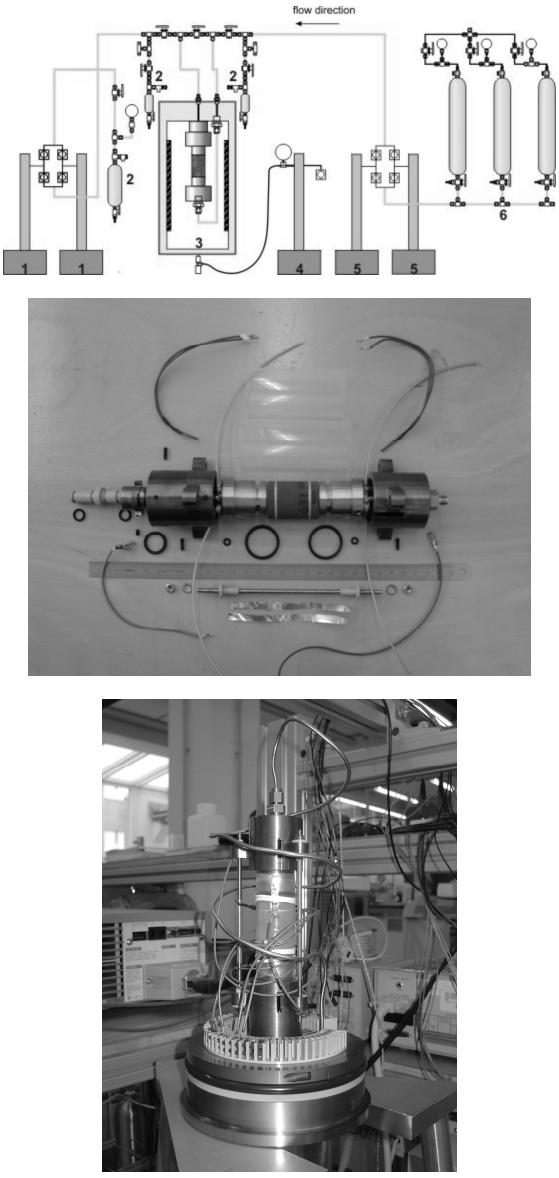

Figure 1: (a, top) General set-up of the apparatus: (1) and (5) down- and upstream pore fluid pumps, respectively; (2) reservoirs for fluid sampling; (3) pressure vessel with internal heater and specimen assembly; (4) confining pressure pump; (6) fluid reservoir. (b, center) Parts of the specimen assembly. Silver rings on the sample serve as potential electrodes for electrical conductivity measurements. (c, bottom) Detail of the mounted specimen assembly

The first well Groß Schönebeck EGrSk3/90 was tested to investigate scenarios of enhancing productivity of thermal fluid recovery from the underground. In order to complete the doublet system a second well GtGrSk4/05 with a total depth of -4198 m has been finished in 2007, followed by three stimulation treatments to enhance productivity (enhanced geothermal system; EGS). For the development of an optimized effective pay zone the new well is inclined in the reservoir section by 48° and was drilled in the direction of the minimum horizontal stress (S_h=288° azimuth) for optimum hydraulic fracture alignment in relation to the stimulated pre-existing well EGrSk3/90. Hence, the orientation of the fractures will be 18° azimuth in the direction of the maximum horizontal stress.

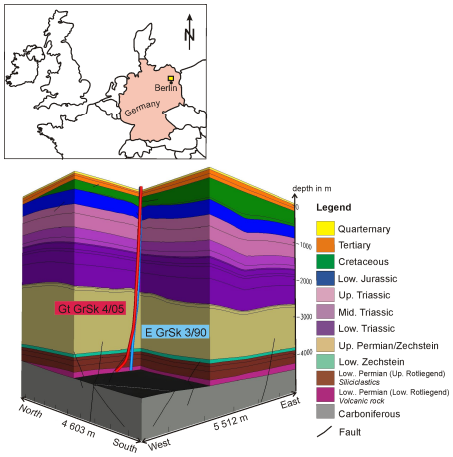

Figure 2: Location of the research drill site (top) and 3D view of the two research wells and the geological horizons; the reservoir is situated in the Lower Permian within a depth of -3850 and -4258 m (bottom)

The reservoir is located in -3850 to -4258 m depth within the Lower Permian of the North East German Basin. The reservoir rocks are classified into two rock units from base to top: volcanic rocks (Lower Rotliegend of the Lower Permian) and siliciclastics (Upper Rotliegend of the Lower Permian) ranging from conglomerates to fine grained sand-, silt- and mudstones.

The fault pattern analysis of a 3D structural model indicates normal to strike slip faulting for the Lower Permian sediments. The formation pore pressure (pp) is 43.8 MPa, determined by p-T logs at stationary conditions of the geothermal target horizon (Legarth et al., 2005). According to the stress relation of normal faulting the effective mean stress (σ_{meff}) was calculated as 42.9 MPa (Blöcher et al., 2008). The temperature at this location follows a normal geothermal gradient and is approximately 150°C. The pore fluid within the formation is of Ca-Na-Cl type with a high salinity (TDS ≈ 265 g/L). Furthermore and in addition to other species, it has a non-negligible degree of mineralization with respect to Fe, Ba and SO_4 with concentrations typically around 67.6 mg/L, 25.5 mg/L, and 51.0 mg/L, respectively.

A detailed description of the geology at this site and the stimulation treatments can be found in Moeck et al. (2008) and Zimmermann et al. (2008), respectively.

3.2 Iceland

High temperature geothermal fields in Iceland, like in other volcanic areas of the world show a particular resistivity structure. Here, a broad resistivity anomaly exists with an up-doming conductive cap covering a resistive core (e.g. Flovenz et al., 1985). The conductive cap consists of volcanic rock with considerable content of conductive alteration minerals, like smectite, that have high cation exchange capacity. The resistivity of the cap decreases with increasing temperature until a core of high resistivity is reached. According to well logging, the transition from the low resistivity cap to the high resistivity core coincides with a change in the mineral alteration, i.e. from smectite to mixed layer clays and chlorite.

Rock samples tested in the present studies originated from three different geothermal fields and five different wells: (1) the Ölkelduháls-field (well ÖJ-1), (2) the Nesjavellir-field (well NJ-17), both in the Hengill volcanic complex near Reykjavik, and (3) the Krafla-field (wells K-2, KH-1, and KH-5) in NE-Iceland.

With decreasing depth the samples display different stages of alteration from the chlorite over the mixed layer clay to the smectite zone. Rock types are hyaloclastites and basalts. All fields are freshwater liquid-dominated with fluids of Na-K-Cl-SO_4 type and low salinity (TDS ≈ 1 g/L).

4. INDIVIDUAL PARAMETERS AND PROCESSES INVESTIGATED

4.1 Pressure Dependence of Rock Transport Properties and Their Interrelations

4.1.1 Motivation

Both permeability (k) and (specific) electrical conductivity (σ) are measured as bulk properties but are in fact defined by the individual pore structure of a rock. This is evident for permeability but is also true for the electrical conductivity as long as the latter is governed by the conductivity of a fluid within the pore space. Furthermore, the pore structure is affected by changes in the state of stress acting on the rock. Both transport properties are therefore dependent on effective stress or, in the lithostatic (isotropic) case, on effective pressure (p_{eff}). Compared to permeability, electrical rock conductivity is significantly easier to measure both in the lab and in situ. Thus, not least for practical reasons, it is desirable to establish a link between both transport properties and to couple both parameters through microstructure-related length scales.

Such approaches have been made repeatedly during the last five decades. Based on geometrical (equivalent channel) models (Wyllie and Rose, 1950; Paterson, 1983; Walsh and Brace, 1984) as well as statistical and percolation concepts (Katz and Thompson, 1986, 1987; Guéguen and Dienes, 1989) a relationship (Eq. 1) is obtained that links both transport properties, where the electrical conductivity is expressed in terms of the formation factor (F):

$$k = c\,L^2\,\frac{1}{F}, \tag{1}$$

where c and L denote a shape factor and a characteristic length scale, respectively. The formation factor F here is defined as the ratio between the electrical conductivity of the fluid (σ_{fl}) at the respective experimental temperature and the measured conductivity of the rock (σ). The physical meaning of both parameters c and L is dependent on the respective model and can vary significantly.

The purpose of this study was to test the predictions of Eq. 1 against original experimental and microstructural data obtained for three different types of sandstone. More specifically, we tested the models proposed by Walsh and Brace (1984), Guéguen and Dienes (1989), and Katz and Thompson (1986, 1987) with shape factors (c) and length scales (L) listed in **Table 1**.

Furthermore, we compared Eq. 1 with an established empirical relationship between k and F (Eq. 2; e.g. Brace, 1977; Walsh and Brace, 1984 and references cited therein) that has been obtained from investigations on the pressure dependence of the coupled transport properties:

$$k = c\,L_E^{\,2}\,\frac{1}{F^r}, \tag{2}$$

Table 1. Parameters of the scaling models investigated. *c*: shape factor; *L*: length scale; *m*: hydraulic radius; V_p: (total) pore volume; A_p: (total) inner pore surface; r_A: average tube radius; w_A: average crack half aperture; l_c: length scale defined by Katz and Thompson (1986, 1987).

Model	c [1]	L [µm]
Hydraulic Radius (Walsh and Brace, 1984)	1/2 (tube) 1/3 (crack)	$m = (V_p/A_p)$
Statistics and Percolation (Guéguen and Dienes, 1989)	1/8 (tube) 8/15 (crack)	r_A (tube) w_A (crack)
Mercury Porosimetry (Katz and Thompson, 1986; 1987)	1/226	l_c

where r denotes an empirical, rock dependent parameter following the notation in Walsh and Brace (1984). The subscript E has been introduced to distinguish between both length scales defined within the respective relationship.

4.1.2 Experimental Procedure

For the experiments three different types of sandstone samples were chosen: (1) Fontainebleau sandstone, a pure quartz arenite, (2) Flechtinger sandstone, a Lower Permian (Rotliegend) sedimentary rock quarried from an outcrop near Flechtingen, Germany, and (3) Eberswalder sandstone, a Lower Permian (Rotliegend) rock cored during drilling of a prospective gas well (Eb2/76) at Eberswalde, Germany. The two Rotliegend samples were chosen for their mineralogical and morphological similarity with the reservoir rocks at the Groß Schönebeck site where cores were no longer available.

To enable electrical conductivity measurements 0.1 molar NaCl-solution was used as the pore fluid. The experiments were performed in the HPT-permeameter described above. To avoid disturbance of the measurement by room temperature fluctuations the experimental temperature was maintained at 40 (± 1) °C.

Both transport properties were measured simultaneously. To investigate the relative changes of both parameters effective pressure ramping was performed by successively increasing and decreasing both confining and pore pressure. The pressures were varied from 10 to 50 MPa (p_c) and 5 to 45 MPa (p_p), respectively. Three full cycles and thus 12 individual ramps were conducted for each sample. In contrast to electrical conductivity which can be determined continuously during pressure ramping, permeability measurements have to be performed stepwise. Depending on the sample permeability 5 to 10 measurements have been taken along each ramp at effective pressure intervals ranging from 2.5 to 15 MPa.

Table 2. Sample properties at starting conditions: confining pressure = 10 MPa; pore pressure = 5 MPa; Temperature = 40°C. φ_s: sample porosity measured by saturation at zero effective pressure; k_0: permeability; σ_0: electrical conductivity; F_0: formation factor.

Sample	φ_s [%]	k_0 [10^{-15} m^2]	σ_0 [mS/cm]	F_0 [1]
Fontainebleau	7.5	20.6	0.113	124.9
Flechtinger	9.0	0.027	0.370	38.1
Eberswalder	4.0	0.0091	0.215	65.6

Subsequent to each test thin sections were prepared. Two on the opposing faces of the specimen and one along the core. The sections were saturated with blue epoxy to allow 2D image analysis to be performed on binary images (Zeiss Axioplan with Axiocam and KSRun). The image analysis program yields the measured pore radius distribution as a function of the (total) cumulative porosity as well as an average pore radius.

In addition, mercury porosimetry (WS2000, Fisons Instruments) was performed after the experiments on broken parts of the samples having a volume of approximately 1 to 2 cm^3 each. This independent method also yields a pore radius distribution of the samples as a function of the (connected) cumulative porosity as well as an average pore radius. In addition, the specific inner surface distribution is calculated from the mercury injection curve.

4.1.3 Results and Discussion

Figures 3a and 3b show the measured normalized permeability and electrical conductivity, respectively as a function of effective pressure. Absolute values can then be obtained from the respective figure and **Table 2**. Both transport properties are sensitive to changes in effective pressure. The sensitivity increases from the Fontainebleau over the Flechtinger to the Eberswalder sandstone. Furthermore, for all sandstones the sensitivity decreases with increasing effective pressure. The percental changes of both transport properties are closely related for the Fontainebleau and the Flechtinger sandstones. In contrast, for the Eberswalder sandstone the decrease in permeability at lower effective pressures is significantly more pronounced than the decrease in electrical conductivity.

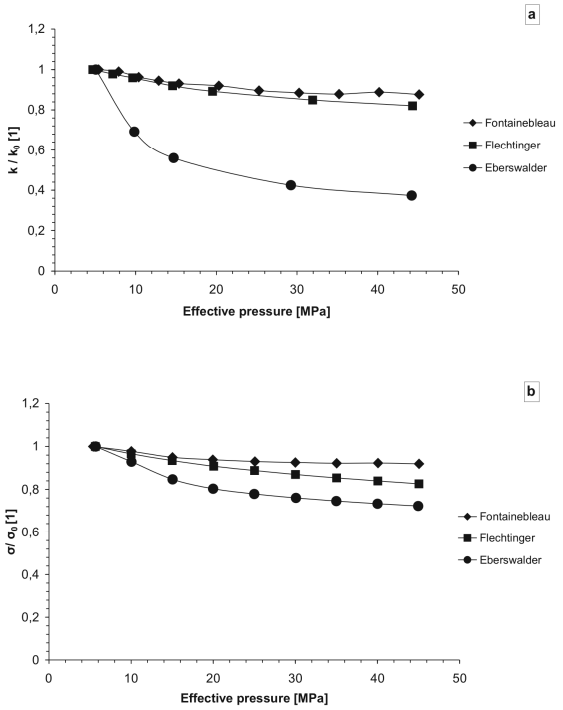

Figure 3: (a) Normalized permeability as a function of effective pressure. (b) Normalized electrical conductivity as a function of effective pressure. Normalization has been performed with the starting permeability (k_0) and starting conductivity (σ_0) in Table 2, respectively

The average pore radius decreases from the Fontainebleau over the Flechtinger to the Eberswalder sandstone. In contrast, the specific inner surface (A_{Hg}) of the Fontainebleau sandstone is significantly smaller than the ones of the two Rotliegend samples. The pore radius distribution from mercury porosimetry (**Figure 4a**) indicates that is due to the narrow distribution and large pore radius of the Fontainebleau sandstone. This contrasts the distribution of the two Rotliegend samples implying significant morphological differences. Their larger specific inner surfaces (**Figure 4b**) are principally due to contributions from pore radii between 0.2 – 2.0 µm.

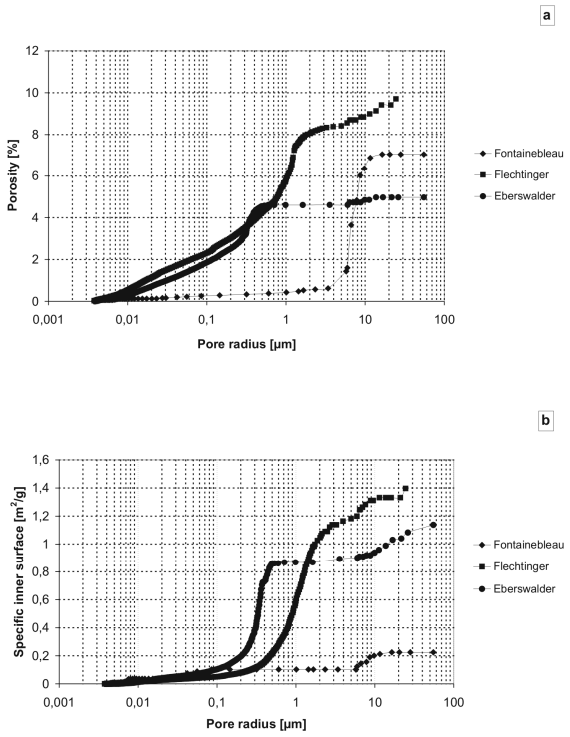

Figure 4: (a) Cumulative porosity and (b) cumulative specific inner surface as a function of the pore radius measured with mercury porosimetry

Testing of the scaling models described above has been performed by permutation of all three parameters measured (permeability, formation factor, and length scale) calculating one property from the two others. It showed that none of the tested models could reproduce any of the experimentally or microstructurally determined parameters adequately within experimental precision. Additionally, there was no clear preference for one of the models as for each of the rocks there was a different model with the closest numerical agreement. It also showed that models that are based on a tube geometry yield better results than crack models, which in this study is solely related to the differences in the shape factor. Furthermore, the compilation demonstrates that the use of the average throat radius as the length scale in the model by Guéguen and Dienes (1989) yields better results than the average pore radius itself.

The observed inaccuracy of the models by Walsh and Brace (1984) and Guéguen and Dienes (1989) might be related to the assumption that both hydraulic and electrical transport follows the same flow paths (David, 1993; Van Siclen, 2002). This implies transport property dependent tortuosities (Walsh and Brace, 1984) and percolation factors (Guéguen and Dienes, 1989). In dependence on the type of rock this reasoning is supported by the mercury porosimetry measurements and furthermore by the analysis of Eq. 1 and Eq. 2 below.

The model by Katz and Thompson (1986, 1987) has its theoretical foundations in the percolation (or critical path-) concept of Ambegaokar et al. (1971) and weights both hydraulic and electrical transport separately through trial solutions (Shante, 1977; Kirkpatrick, 1979) before connecting the constituent equations to yield Eq. 1. A reexamination of their model implied that principally the included shape factor $c = 1/226$ is in fact not a constant but a rock dependent adjustable parameter yielding incorrect results with respect to the experimental data.

The application of Eq. 1 for effective pressures other than zero is strictly only permissible when the concurrent evolution of the rock microstructure (respectively the characteristic length scale) is known. Eq. 2, in contrast, is obtained when both k and F measured during pressure ramping are plotted against each other on a logarithmic scale. The experiments then yield sample dependent parameters r and ($c\ L_E^2$) as the slope of the linear fit to the data and the intersection with the y-axis, respectively. The empirical parameter r took values between 1 and 3 in agreement with previous studies. The parameters c and L_E^2 cannot be derived separately from the experiments but have to be calculated from the model of choice. L_E, in this empirical approach, is thus a parameter with no true microstructural meaning and has lost its character as a natural length scale.

This becomes evident when the product ($k\ F$) normalized by the starting values ($k_0\ F_0$) is plotted as a function of effective pressure (**Figure 5a**) and is compared to the pressure dependence of the product ($k\ F^r$) normalized by the starting values ($k_0\ F_0^r$) (**Figure 5b**). Any departure of the graphs from a value of 1 (Figure 5a) indicates a pressure dependence of the product ($k\ F$) and thus ($c\ L^2$) in Eq. 1. In Figure 5b all graphs remain close to 1 as the product ($c\ L_E^2$) is a constant by definition as outlined above. Here, the pressure dependence of the microstructure is implicitly contained within the empirical parameter r. It finally showed that r can vary with pressure, specifically when the permeability of the sandstone is dominated by crack porosity. We interpret the empirical parameter r as a measure of the relative effect of pressure changes on the linked transport properties. In turn, it can also be viewed as a qualitative indicator for the degree of coincidence of hydraulic and electrical flow paths.

This study is documented in detail in Milsch et al. (2008b).

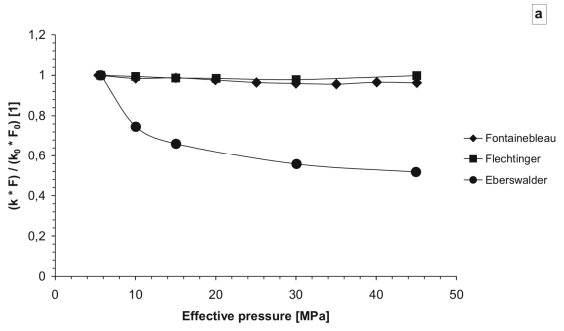

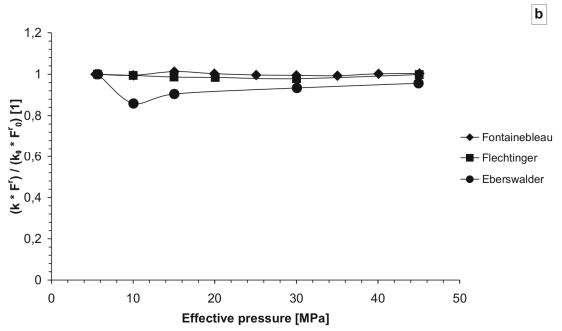

Figure 5: (a) Normalized product ($k\ F$) as a function of effective pressure. Normalization has been performed with the respective starting values (k_0 and F_0) in Table 2. (b) Normalized product ($k\ F^r$) as a function of effective pressure with the parameter r being sample dependent

4.2 Effect of Dissolution-Precipitation Reactions on Rock Permeability

4.2.1 Motivation

In the course of reservoir stimulation and exploitation related to the Groß Schönebeck site the local thermodynamic equilibrium of the formation is disturbed. This might induce a number of fluid-fluid- and fluid-rock interactions potentially leading to permeability damage:

(1) During reservoir stimulation by a water-frac, the formation fluid is displaced by oxygen-rich well water. This possibly causes the precipitation of iron hydroxides (Seibt, 2000 and references cited therein). During the former procedure the temperature in the proximity of the injection well can be as low as 30°C.

(2) After passing the binary power plant cycle the cooled formation fluid might become oversaturated with respect to Ba^{2+} and SO_4^{2-}. Thermodynamic calculations (CHEMEQ) with the typical in situ concentration range indicated a positive saturation index (SI > 0) for temperatures below 70°C (J. Bartels, personal communication, 2006). As this corresponds to the approximate fluid reinjection temperature, formation damage due to baryte precipitation is potentially promoted (Kühn et al, 1997; Dunn et al., 1999).

(3) Finally, any alteration of fluid saturation with respect to the different ionic species of the rock minerals (e.g. Si) might induce dissolution-precipitation reactions within the formation in the course of fluid production (Aharonov et al., 1998; Tenthorey et al., 1998).

In contrast, an effect of clay swelling on the rock permeability (e.g. Omar, 1990) in the present case is not to be expected as the rock does not contain the relevant clay minerals. The preceding conditions and processes defined the experiments performed in this study. This study was conducted under realistic conditions regarding rock- and fluid type, combinations of confining- and pore pressures, flow-rates as well as temperatures. The principal physical parameter investigated in the present study was the rock permeability. The latter was complemented by continuous measurements of the electrical sample conductivity as well as a chemical analysis of the pore fluid in regular time intervals.

4.2.2 Experimental Procedure

The samples tested came from a prospective oil and gas well near Eberswalde / Germany (Eb 2/76). They were chosen for their mineralogical similarity with the aquifer rocks at the close by Groß Schönebeck site where, again, cores were no longer available. The specimens are Lower Permian (Rotliegend) sandstones of the Havel subgroup originating from a depth of approximately 4150 m. The rock is an arcosic litharenite and consists mainly of quartz (65 vol%). The feldspar content is less than 15 vol%. Rock fragments are contained by approximately 20 vol% and are mainly of volcanic origin. Illite and chlorite are the dominant clays. For the experiments cores were taken parallel to the bedding. Two specimens labelled ebe05-3 and ebe05-4 were tested.

The fluids used were a 0.1 molar NaCl solution (sample ebe05-3) and a synthetic Ca-Na-Cl type formation fluid (sample ebe05-4). The fluid contained 99 g NaCl and 206 g $CaCl_2 \cdot 2H_2O$ per liter distilled water and thus a total amount of dissolved solids (TDS) of 265 g/L.

The experiments were conducted under hydrostatic conditions in the HPT-permeameter described above. After assembly, the specimens were subjected to a confining- and pore pressure of 10 and 5 MPa and a temperature of 30°C, respectively defining the starting conditions. Given a full stroke volume of 265 mL the active upstream pore fluid pump was refilled approximately once per day with the respective fluid. The flow was unidirectional and repeated pumping of the same fluid was not performed.

The long-term flow-through experiment with sample ebe05-4, which we will focus at in the following, had a total duration of 186 days. The flow-rate was 0.1 mL/min and the test was performed at a constant confining- and pore pressure of 50 and 5 MPa, respectively. After confining pressure increase to 50 MPa the temperature was maintained at 30°C for three days and was then increased to 150°C. After 30 and 83 days the flow was stopped and the sample was maintained at stable p-T conditions for 45 and 81 days respectively. After these holds flow was resumed for approximately 7 days each.

Subsequent to this first experimental stage the fluid was enriched with progressively increased concentrations of Ba^{2+} and SO_4^{2-} ions by adding specific amounts of 0.1 molar $BaCl_2$ and Na_2SO_4 solutions to the synthetic formation fluid. Three different concentrations $n(Ba^{2+}):n(SO_4^{2-})$ [n in mM/L] were tested: (1) 0.19:0.19; (2) 0.19:0.57, and (3) 0.38:1.14. This covers the in situ Ba^{2+} concentrations and $n(Ba^{2+}):n(SO_4^{2-})$ ratios of the Groß Schönebeck formation fluid which are in the range of 0.19 to 0.44 mM/L and 1:1 to 1:3, respectively. This flow-through test took 7 days and was performed at a temperature of 60°C.

The fluid was then exchanged at 150°C against tap water acidified to pH5 with acetic acid and the temperature was then, again, decreased to 60°C and then further to 30°C. The flow with tap water was maintained for 5 days. At the end of this experimental stage the tap water was finally exchanged against the original synthetic formation fluid and the temperature was increased to 150°C to establish the starting conditions for comparison.

For sample ebe05-4 the total amount of fluid that had transversed the sample during 60 days of flow was 8.6 L. During both stages of this experiment a total of 30 fluid samples were taken, generally one every second day during

times of flow. The samples contained approximately 150 mL of fluid each. Immediately after release the fluid pH and redox potential Eh were measured at ambient p-T conditions (WTW Multi 340i with Mettler-Toledo probes InLab 412 (pH) and InLab 501 (Eh)).

The fluid samples were then chemically analysed for cation and anion concentrations of Fe, Mn, Al, Zn, Cu, Pb, K, Si, Ba, and SO_4, respectively. Besides for Fe and Mn which were analysed photometrically chemical analysis was performed by either GF-AAS (Graphite Furnance Atomic Absorption Spectrometry; Al, Zn, Cu, Pb) or by ICP-MS (Inductively Coupled Plasma Mass Spectrometry; K, Si, Ba, and SO_4 through S) at VKTA Rossendorf e.V. Here, the detectable minimum concentrations, taking dilution into account, were 50 µg/L (Al, Zn), 10 µg/L (Cu, Pb, K), 60 µg/L (Si), 5 µg/L (Ba), and 1500 µg/L (SO_4), respectively.

4.2.3 Results and Discussion

The evolution of permeability during the first stage of this experiment is shown in **Figure 6**. The permeability decrease after start from $4.9 \cdot 10^{-15}$ to $2.0 \cdot 10^{-15}$ m^2 is due to a confining pressure increase from 10 to 50 MPa. During the first 26 days of flow the permeability remained constant at $2.2 \pm 0.8 \cdot 10^{-15}$ m^2. The two longer holds were introduced for comparison by allowing a chemical equilibration of the fluid with the rock. After flow was resumed the permeability had decreased by approximately 50 % to $1 \pm 0.1 \cdot 10^{-15}$ m^2. In contrast, it remained nearly constant for the remainder of the experiment.

The **Figures 7 and 8** show the temperature and permeability, respectively as a function of time in the course of the second stage of this experiment. For each of the three different Ba^{2+} and SO_4^{2-} concentrations the flow was maintained for two to three days. As the principal result, neither a change in temperature nor the different fluid exchanges affected the sample permeability which remained constant at approximately $1 \pm 0.1 \cdot 10^{-15}$ m^2.

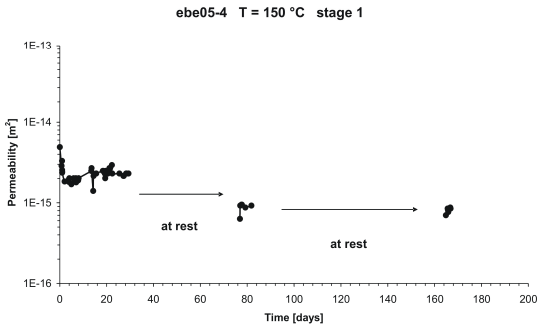

Figure 6: Sample ebe05-4, stage 1. Permeability as a function of time

The formation fluid pH before the onset of the experiment was 5.5 at 21.9°C. The recovered fluid samples had pH-values in the range of 5.1 and 6.6 at 20.0°C with no systematic trend. The redox potential measurements yielded inconsistent results. Fe and Mn, both measured photometrically, yielded concentrations of 1.72 ± 0.87 mg/L and 1.76 ± 0.78 mg/L, respectively. The former was the highest right at the beginning of the test after the temperature had been increased to 150°C and slightly decreased in the course of the experiment. For the Mn concentration no systematic trend was observed. The chemical fluid analysis indicates that ionic species of K, Cu, Zn and Pb that have been residually preserved within the sample after initial coring become easily dissolved and flushed-out after flow has been started. No dissolution of Al was observed despite the presence of K-feldspar as well as illite and chlorite. Si maintained an approximately constant (equilibrium) concentration of 30 ppm (stage 1) regardless of the flow situation. The former appears to be affected by the presence of Ba^{2+} and/or SO_4^{2-} ions when the latter were introduced artificially (stage 2). An approximately constant $n(Ba^{2+}):n(SO_4^{2-})$ ratio of 1:2.2 ± 10 % was observed during stage 1 and thus prior to the enrichment of the formation fluid with these species. This indicates the preservation of baryte precipitates after initial core recovery or the presence of smaller amounts of baryte cement. Consequently, no effect of precipitation was observed during stage 2 for a molar ratio of 1:1. Despite a progressive relative depletion in Ba^{2+} ions, the SO_4^{2-} concentration measured indicates that baryte precipitation can also be excluded for the lowest $n(Ba^{2+}):n(SO_4^{2-})$ ratios investigated in the present study.

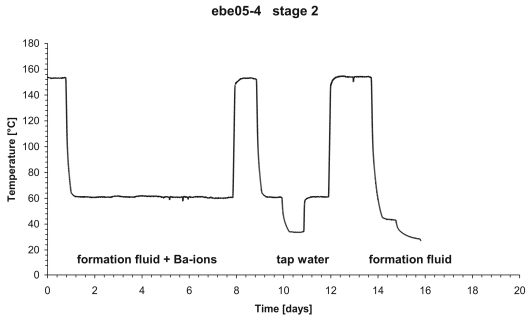

Figure 7: Sample ebe05-4, stage 2. Temperature as a function of time during fluid exchange

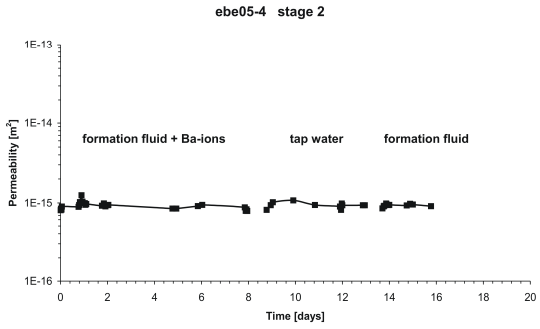

Figure 8: Sample ebe05-4, stage 2. Permeability as a function of time during fluid exchange

Based on the measurements performed it is finally concluded that during neither long-term experiment with an isochemical fluid composition any significant alteration of the transport properties had occurred. Also during stage 2 (sample ebe05-4) no further change in sample permeability was observed. For baryte precipitation this is evidently due to an insufficient Ba^{2+} and SO_4^{2-} concentration. In addition, precipitation experiments (A. Seibt, 2006, personal communication) indicate that baryte nucleation is significantly retarded when the fluid is in motion. For the fluid exchange against tap water this indicates that an effect on the rock transport properties is only to be expected when the replaced formation fluid contains a significant amount of ionic species to be oxidized (e. g. Fe^{2+}).

A detailed documentation of this study can be found in Milsch et al. (2009).

4.3 Temperature Dependence of Electrical Rock Conductivity and Seismic Wave Velocities

4.3.1 Motivation

Contrary to oil and gas exploration where reflection seismic surveys are the main exploration method, no similar standard exploration methods exist for high temperature geothermal exploration. The on-site conditions are highly variable and the exploration technology has to be tailor-made for each geothermal field. In exploring for high temperature fields, reflection seismic surveys are of limited use due to the structural irregularities. The most common geophysical methodology involves mainly different types of resistivity soundings supplemented with other methods like gravity, magnetic and passive seismic surveys. In order to draw reliable conclusions about geothermal properties from the results of geophysical surveys a firm knowledge of the temperature behaviour of parameters like resistivity and seismic wave velocity is necessary.

More specifically and in connection with the background given in Section 3.2, changes in mineralogy were reported to occur at temperatures close to 230°C in Icelandic geothermal fields (Kristmannsdóttir, 1979). However, the change in resistivity appears to be frozen-in via the mineral alteration, i.e. in case the reservoir has cooled down the boundary between low and high resistivity persists and does not indicate temperatures exceeding 230°C anymore. It follows that the top of the high resistive core represents a surface where the temperature once has reached 230°C but it might have cooled down since. For geothermal exploration it is important to be able to distinguish between these two cases and find out if the resistive core has cooled down. One way to move forward is to learn more about the temperature behaviour of resistivity, both within the smectite and chlorite alteration zone. For that purpose, laboratory measurements at in situ conditions on core samples from various zones of mineral alteration are important, to determine if there is a way to make any distinction between reservoirs that have cooled down and those who have not.

The two main conduction mechanisms in water saturated rocks are pore fluid conduction and interface conduction. As a first approximation the two mechanisms act in parallel according to the (modified) Waxman-Smits equation:

$$\sigma_0 = \frac{\sigma_f}{F} + \sigma_s, \tag{3}$$

where σ_0, σ_f, σ_s and F are bulk conductivity, pore fluid conductivity, interface conductivity, and formation factor, respectively (Rink and Schopper, 1976).

Fluid conductivity, σ_f, for temperatures below 150°C is linearly dependent on temperature:

$$\sigma_f(T) = \sigma_f(T_0)[1 + \alpha_f(T - T_0)], \tag{4}$$

where T_0 is a reference temperature and α_f is a temperature independent coefficient. The value of α_f is assumed to be 0.023/°C for T_0 = 25°C (Revil et al., 1998). Because of the changed behaviour of density, viscosity and dielectric permittivity of water for temperatures above 150°C, which affects the mobility of free charges, the conductivity diverges from linearity above this temperature limit and normally decreases with increasing temperature above 250°C (Ucok et al., 1980).

Interface conductivity is dependent on the surface area of pores, the surface charge density, the valence and mobility of surface ions, temperature, and acidity (pH). For temperatures below 200°C, however, also interface conductivity, σ_s, can be described by a linear relationship with temperature:

$$\sigma_s(T) = \sigma_s(T_0)[1 + \alpha_s(T - T_0)], \tag{5}$$

where, as before, T_0 is a reference temperature and α_s is a temperature independent coefficient. Revil et al. (1998) determined a value of α_s = 0.040/°C for T_0 = 25°C. In general, surface conductivity is believed to be more temperature dependent than pore fluid conductivity (Revil et al., 1998).

There is a clear difference in conductivity between rocks in the smectite or chlorite alteration zone, according to field measurements. The cation exchange capacity (CEC), which is the quantity of exchangeable cations on a negatively charged mineral surface, is not the same for these two clay minerals: For smectite the CEC is 0.8-1.5 meq/g (Ellis, 1987) and for chlorite it is 0.01 meq/g (Thomas, 1976), possibly explaining the great difference in conductivity between the two mineral alteration zones.

4.3.2 Experimental Procedure

All measurements were made at the GFZ in the HPT-permeameter described above. The measured samples all originated from Icelandic boreholes. All samples were kept dry at room conditions since their drilling, except sample K40 which was kept submerged in fluid. An overview of the samples used in this investigation can be found in **Table 3**. With exception of sample K40, the fluids of all other specimens were synthetically prepared. This was achieved by dissolving specific amounts of reagent grade NaCl, KCl, Na_2SO_4, and K_2SO_4 salts in distilled water. The specific concentrations chosen were based on fluid analyses of samples taken at the respective geothermal site and reflect the principal in situ chemical compositions. A total of 7 samples were heated in steps of 25°C or 50°C in the temperature range of 25°C to 250°C, keeping confining and pore pressure constant at the respective in situ condition. Meanwhile, the temperature at the sample, pore and confining pressure, and electrical conductivity of the sample were recorded continuously. When equilibrium in temperature and conductivity had been reached for each step both impedance in the frequency range 0.01 Hz to 100 kHz and P-wave velocity were measured in addition.

Sample no.	Location	Well no.	Material	Alteration zone	Sample depth (m)	In-situ temperature (°C)	Estimated in-situ fluid conductivity at 25°C (mS/cm)	Porosity (%)	Density (g/cm³)	Confining pressure (MPa)	Pore fluid pressure (MPa)
2B	Hengill	ÖJ-1	Hyalo-clastite	Chlorite / Epidote	794.5	200	0.808	14.6	2.59	18.5	8.0
3A	Hengill	ÖJ-1	Hyalo-clastite	Chlorite / Epidote	795.0	200	0.808	20.7	2.46	15.0	8.0
K40	Krafla	KH-5	Basalt	MLC / Chlorite	537.5	120	-	13.2	2.29	13.5	5.0
58	Krafla	KH-1	Basalt	Smectite / MLC	187.5	160	0.780	20.0	2.37	5.0	1.9
FTBS12	Fontaine-bleau	N/A	Sand-stone	No alteration	-	-	(10.8)	12.5	2.29	10.0	5.0

Table 3. Sample properties (Sections 4.3, 4.4, 4.5), MLC: mixed layer clays.

4.3.3 Results and Discussion

The general behavior of conductivity with respect to temperature was similar for all samples tested. As an example we present the data for one particular sample (2B). Temperature and conductivity as a function of time are depicted in **Figure 9**. Conductivity as a function of temperature is shown in **Figure 10**. Note the apparent transient conductivity increase at 150°C, which indicates changes in the intrinsic sample properties (Section 4.4).

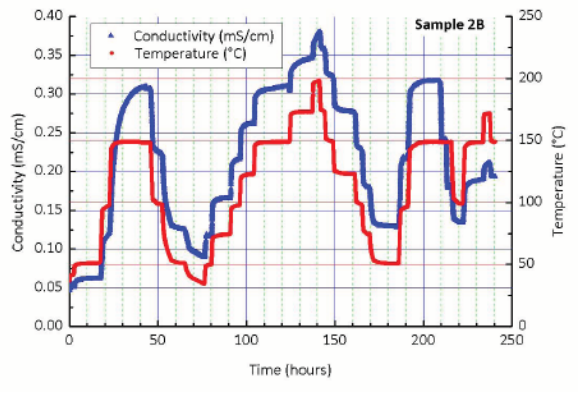

Figure 9: Conductivity and temperature as a function of time. Example: sample 2B.

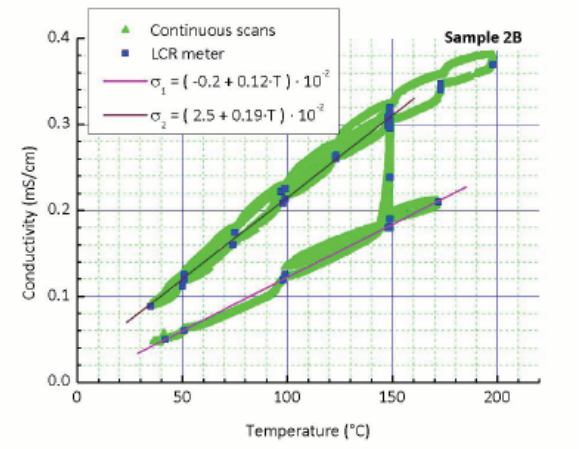

Figure 10: Conductivity as a function of temperature, showing measurements made both in continuous scans and with an LCR-meter. Example: sample 2B

The linear relation between conductivity and temperature in the range 50-170°C is evident, both before and after the change in conductivity. At temperatures above 170-200°C the conductivity becomes less and less temperature dependent. If both conduction mechanisms contribute, the slope α of the curve $\sigma(T)/\sigma(T_0)$ takes on a value somewhere between α_f and α_s, i.e. $\alpha = \dfrac{\alpha_s \sigma_s(T_0) + \alpha_f \sigma_f(T_0)/F}{\sigma(T_0)}$.

For T_0 = 25°C we obtain values in the range α = 0.027-0.28 /°C, i.e. all higher than α_f = 0.023 /°C. This could indicate that pore fluid conduction is dominated by interface conduction both in the smectite zone and the chlorite zone, although samples 2B and 3A from well ÖJ-1 are most likely a mixture of interface and pore fluid conduction after the conductivity change at 150°C (α = (0.027±0.003) /°C). We conclude that there is no definite difference in conduction mechanisms between the smectite zone and the mixed layer clays / chlorite zone. Therefore we assume that the much lower CEC of chlorite compared to smectite is the most likely cause of the clear conductivity decrease between the smectite and chlorite zones in geothermal HT-fields.

Finally, the measurements of P-wave velocities indicate a systematic decrease by 5 to 15 % with temperature for all samples. Before the observed transient change in conductivity the velocities were slightly higher than afterwards at the respective temperature. P-wave velocities were in the range of 4.4 km/s (25°C) and 3.4 km/s (250°C).

A complete documentation of this study can be found in Kristinsdóttir et al. (in review). The ultrasonic data is documented and analysed in detail in Jaya et al. (in review).

In an ongoing study, similar experiments on conductivity and ultrasonic wave velocities are conducted on Italian samples from the Anqua and Radicondoli wells in the Travale geothermal test site.

4.4 Evolution of Electrical Rock Conductivity in a Fluid-Rock Disequilibrium

4.4.1 Motivation

As indicated in Section 4.3 electrical conductivity showed a transient behavior when the sample was first heated to 150°C. This implies a change in the samples' intrinsic properties as a result of a fluid-rock disequilibrium until a thermodynamically stable state is reached with respect to the actual p-T-X conditions. An investigation of this effect is of particular importance as reservoir states of equilibrium are always disturbed during stimulation procedures and as fluid is produced. As a consequence, results of resistivity logging will be time dependent as well and the obtained data has to be interpreted accordingly. Also, so measured approaches to equilibrium could potentially be interpreted as saturation states of the pore fluid. A disturbance of fluid-rock equilibria, e.g. by cooling during energy production, might result in mineral precipitation and consequently in permeability damage in the near-bore region of the injection well or even deeper within the formation.

4.4.2 Experimental Procedure

During the experiments described in Section 4.3 two of the samples (2B and K40) were flushed with fresh pore fluid to measure permeability. Measurements were made at 40°C before the temperature was raised for the first time and then repeatedly during each temperature cycle at 150°C, after conductivity had stabilized. The flow rate was Q = 25 µL/min for sample K40 and Q = 50 µL/min for sample 2B.

4.4.3 Results and Discussion

The permeability decreased considerably as the samples were heated from 40°C to 150°C, i.e. during the conductivity hysteresis: from 9.3 to 5.5 µD (K40) and 25.4 to 21.8 µD (2B). The reason for this decrease, at present, remains unresolved. At constant temperature (150°C) the permeability of both samples remained approximately constant within experimental resolution, i.e. k = (5.3±0.2) µD for sample K40, and k = (18.7±0.6) µD for sample 2B.

During every permeability test the conductivity decreased at 5-10 µS/cm·h for sample K40 and 8-12 µS/cm·h for sample 2B, except in the last measurement (2B) when the decrease was as high as 72 µS/cm·h. This last conductivity decrease in sample 2B is shown in red on **Figure 11**. The final conductivity value after this decrease replicated exactly the one before the transition at 150°C. Afterwards,

the temperature was decreased and increased again to measure the actual σ-T relation.

The transient conductivity behaviour around 150°C and its reversibility have yet to be explained. However, the temperature coefficient α decreased for every sample during the transition which indicates that the conductance is more associated with the fluid conductivity than before. Also, the fluid in the system before the measurements had a conductivity of σ = 970 µS/cm. After the measurements the conductivity of the fluid in the downstream pump was σ = 1280 µS/cm.

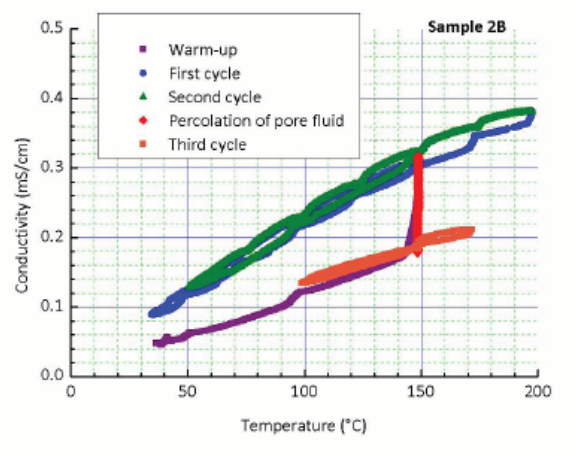

Figure 11: Conductivity as a function of temperature (continuous scans), with each heating cycle shown in different color. Example: sample 2B

Based on these observations it is implied that the transient conductivity behavior is due to some flow of ions over the boundary between the (clay) minerals or the Stern layer and the pore fluid, more precisely, that there is some uncompensated exchange of ions or mineral dissolution. The result is that a larger proportion of the ions that contribute most to the conductivity are in contact with free fluid. Hence, when fresh fluid flows through the sample these additional ions are washed out and the sample conductivity decreases.

The data related to this section is documented in more detail in Kristinsdóttir et al. (in review).

In an ongoing study, the former effects are investigated for rocks originating from or related to sedimentary geothermal reservoirs (Schepers and Milsch, 2009).

4.5 Petrophysical Signature of a Water-Steam Phase Transition within the Pore Space

4.5.1 Motivation

During production from high temperature geothermal reservoirs the pore pressure decreases in response to the mass withdrawal. This results in the onset of boiling often followed by formation of a steam cap above the production zone. The steam cap can both be a target for energy production as well as a source of potential hazards if the pressure in the steam cap exceeds the weight of the overburden. For both reasons it is therefore of particular importance to develop methods to detect and map the extent of such steam caps. As the electrical conductivity of steam is much lower than that of liquid water electrical exploration methods might be particularly suitable if the conductivity contrast at the field scale is high enough.

The overall effect of boiling on electrical conductivity within geothermal reservoirs is poorly constrained although it can be expected that conductivity will decrease if boiling starts. In contrast to this likely scenario for fluid dominated electrical conductivity, the direct effect of vaporization on surface conduction in the pores is, so far, unknown.

Based on the Young-Laplace concept of capillarity (e.g. Bear, 1988) Roberts et al. (2001a) proposed a model for a finely porous medium, where pore fluid vaporization would be heterogeneous as pore pressure is decreased, because of the effect of capillary suction. For a finely porous medium, vaporization proceeds when the pore pressure is:

$$p_{pore} \leq p_{boil} + p_{cap}\,, \tag{6}$$

where p_{pore}, p_{boil}, and p_{cap} are the pore pressure, boiling (vapor) pressure, and capillary pressure, respectively. At least for fluid dominated conduction, the signature of vaporization with respect to electrical conductivity will therefore be dependent on the individual rock microstructure.

4.5.2 Experimental Procedure

The experiments were conducted at the GFZ in the HPT-permeameter described above and subsequent to the investigations reported in Section 4.3 and 4.4. Again, the measurements were carried out on the four volcanic rock samples from Iceland, two basalts (58 and K40) and two hyaloclastites (2B and 3A). One sample of sandstone from Fontainebleau, France (FTBS12) was added to the experimental program as a reference (Table 3). The fluid used for the Fontainebleau sandstone was a 0.1 molar NaCl synthetic solution having an electrical conductivity of 10.8 mS/cm at 25°C.

During the experiments both temperature (nominally 150°C) and confining pressure were kept constant. In contrast, pore pressure was decreased to allow vaporization of pore fluid in a controlled manner. The downstream pore fluid pump was retracted at a constant rate so that the total volume of the pore fluid system was steadily increased. As both sides of the sample were connected during this procedure, the nominal pore pressure was equal at either face of a specimen. The pore fluid pumps were kept at room temperature and vaporization was restricted to the hot zone of the pore fluid system located within the pressure vessel. During the experiments the electrical conductivity, the pore pressure, the volume of the pore fluid pump and the sample temperature were continuously monitored.

4.5.3 Results and Discussion

For all samples, a continuous conductivity decrease was observed as the volume of the pore fluid system was increased progressively. The total conductivity decrease during vaporization was generally 1 to 2 orders of magnitude and thus significant. Besides for sample 58 where the measurement was terminated earlier, the electrical conductivity ultimately reached a minimum.

In contrast but also for all samples, there was a discontinuous decrease in pore pressure. Initially, as the volume of the pore fluid system is increased, the pressure dropped rapidly due to elastic relaxation. Then, at the boiling point, an approximately constant pore pressure level was maintained. Finally, the pore pressure continuously decreased again.

The relationship between the evolution of both electrical conductivity and pore (vapor) pressure was observed to be sample dependent. If capillarity is the only reason, differences in pore pressure evolution then would reflect differences in sample microstructure in terms of the individual pore radii distributions. Following the procedure in Roberts et al. (2001a) one can calculate the minimum pore (capillary) radius R related to vaporization by the maximum capillary pressure observed ($p_{cap} \approx$ (-) 0.25 MPa at 150°C):

$$p_{cap} = -2\gamma \cos\theta / R, \quad (7)$$

where γ and θ are surface tension of the wetting fluid (water; $5.2 \cdot 10^{-3}$ Pa m; Weast, 1984) and wetting angle ($\approx$ 0; Roberts et al., 2001a), respectively. One obtains $R \geq 42$ nm, which indicates that virtually all pore size classes were affected by vaporization in the present experiments.

An important conclusion that can be drawn is the amount of vapor required to reduce the electrical conductivity to a minimum with respect to the individual sample porosity. In **Figure 12** one notices that for all samples 5 ± 1 mL of fluid have to be drained before the electrical sample conductivity becomes affected. This volume relates directly to the free fluid volume (e.g. in tubings) located at 150°C inside the pressure vessel. For all but one sample (58) the behavior, then, is similar. The electrical conductivity decreases to only about 5 ± 1 % of its starting value. Furthermore (excluding 58), 7 ± 2 mL of fluid have to be drained from the sample until the minimum electrical conductivity is reached. The total (connected) pore volume of the samples is 3.5 (FTBS12), 3.7 (K40), 4.1 (2B), 5.7 (58), and 5.9 (3A) mL. The ratio between the drained fluid volume and the total pore volume is 1.5 (FTBS12), 2.5 (K40), 1.3 (2B), 3.1 (58), and 1.0 (3A), thus approximately 2.0 ± 1.0 times the relevant pore volume. Due to fluid condensation outside the vessel the drained fluid volume in fact directly reflects the transformed liquid volume contained within the pore fluid system and thus the pore space.

This balance then allows a classification of the rocks. Samples 3A, 2B, and FTBS12 display a very similar conductivity signature. Here, every part of drained volume larger than the pore volume can well be attributed to smaller pores and/or a broader pore size distribution. The excess volume then reflects the vapor expansion related to a pressure decrease necessary for further vaporization. For sample 58, in contrast, the excess volume at the conductivity minimum was comparatively large. This suggests that the curve shapes in Figure 12 could also be indicative of the respective dominating conduction mechanism as vaporization proceeds. Electrical conduction in sample FTBS12 is definitely fluid dominated for the given fluid salinity (Milsch et al., 2008b). This applied to samples 3A and 2B indicates that conduction during vaporization in hyaloclastites emanating from the chlorite alteration zone should be fluid dominated as well, even for pore fluids of low salinity as in the present case. Sample K40, a basalt containing mixed-layer clays, then would display a transition from fluid to surface conduction at a later vaporization stage. Finally and for the present fluid composition, conduction in sample 58, a basalt from the smectite alteration zone, is supposed to be surface dominated. In this case, the decrease in electrical conductivity upon continuous fluid drainage should be related to a progressive destruction of the conductive layer on the mineral surfaces rather than to the phase transformation within the pore space itself. The concurrent evolution of electrical conductivity and pore pressure, in this case, would be largely unrelated. This finally suggests that variances in the respective conduction mechanism yield different electrical signatures as vaporization proceeds.

Finally, at the observed conductivity minimum it can be assumed that apart from retained water on grain surfaces or in ultra-small pores all samples can be considered dry. Therefore, samples with fluid dominated electrical conduction are suggested to approximately quantify their respective liquid-vapor saturation via the measured electrical conductivity signature. The exact phase distribution during vaporization, however, remains unresolved.

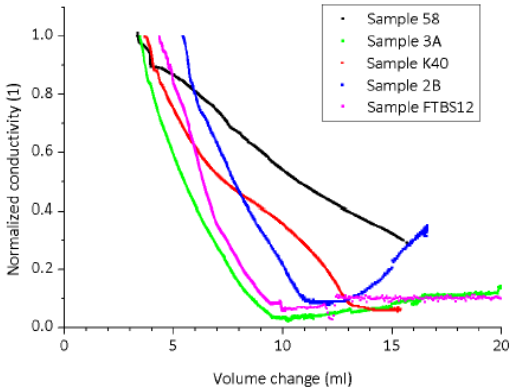

Figure 12: Normalized electrical conductivity as a function of volume change in the pore pressure system. The conductivity normalization was performed with the respective starting value right before the initiation of boiling within the pore space

A detailed documentation of this study can be found in Milsch et al. (in review).

CONCLUSIONS

Two identical flow-through apparatuses have been set-up to simulate p-T-X conditions related to deep geothermal reservoirs. Their long-term performance was successfully tested for confining pressures, pore pressures and temperatures of 100 MPa, 50 MPa and 200 °C, respectively, thus exploring stress-isotropic upper crustal in situ conditions at up to 5 km depth including the respective temperatures for a normal geothermal gradient. Highly saline pore fluids can be used. In addition, four important rock physical parameters (permeability, electrical conductivity as well as P and S wave velocities) can be determined simultaneously. Continuous flow experiments, so far, have been performed over a maximum of six months. Stable physical conditions have thus been maintained over periods that are significantly longer than those usually attained in conventional laboratory based rock physical testing.

Scientifically, the usage of the devices is focused on the evaluation of risk potentials in exploration and exploitation of deep geothermal reservoirs regarding sustainable production. Particularly, the investigations presented above addressed possible effects of fluid-rock interactions on the transport properties of a reservoir host rock. Also, the pressure and temperature dependence of rock properties as well as effects of phase changes within the pore space were characterized in several independent studies. The investigations were conducted both site specific and process

oriented. We presented evidence that laboratory based research is a valuable complement to both field and numerical studies on the long-term evolution of geothermal reservoirs.

ACKNOWLEDGEMENTS

Financial support was provided by the German Federal Ministry for the Environment, Nature Conservation, and Nuclear Safety under grant BMU 0329951B and the European Commission under the 6th Framework Programme of the European Union.

REFERENCES

Aharonov, E., Tenthorey, E., and Scholz, C. H.: Precipitation sealing and diagenesis: 2. Theoretical analysis. J. Geophys. Res. 103 (B10), 23969-23981 (1998).

Ambegaokar, V., Halperin, B.I., and Langer, J.S.: Hopping conductivity in disordered systems. Phys. Rev. B 4, 2612-2620 (1971).

Archie, G.E.: The electrical resistivity log as aid in determining some reservoir characteristics. Trans. Am. Inst. Mech. Eng. 146, 54-61 (1942).

Bear, J.: Dynamics of fluids in porous media. Dover Publ., Inc. Mineola, NY (1988).

Blöcher, G., Moeck, I., Milsch, H., and Zimmermann, G.: Modelling of pore pressure response due to hydraulic stimulation treatments at the geothermal research doublet EGrSk3/90 and GtGrSk4/05 in summer 2007. Proceedings, 33rd Workshop on Geothermal Reservoir Engineering, Stanford University, Stanford, California, SGP-TR-185 (2008).

Blöcher, G., Zimmermann, G., and Milsch, H.: Impact of poroelastic response of sandstones on geothermal power production. Pure appl. geophys. 166, 1-17, doi 10.1007/s00024-009-0475-4 (2009).

Brace, W.F.: Permeability from resistivity and pore shape. J. Geophys. Res. 82 (23), 3343-3349 (1977).

Civan, F.: Reservoir formation damage – Fundamentals, Modelling, Assessment, and Mitigation. 1st Ed., Gulf Publ. Co., Houston, TX, and Butterworth-Heinemann, Woburn, MA, 742 p. (2000).

Darcy, H.: Les fontaines publique de la ville de Dijon. Dalmont, Paris (1856).

David, C.: Geometry of flow paths for fluid transport in rocks. J. Geophys. Res. 98, 12267-12278 (1993).

Dunn, K., Daniel, E., Shuler, P. J., Chen, H. J., Tang, Y., and Yen, T. F.: Mechanisms of surface precipitation and dissolution of baryte: A morphology approach. J. Colloid Interf. Sci. 214 (2), 427-437 (1999).

Ellis, D.V.: Well Logging for Earth Scientist. Elsevier, New York (1987).

Flovenz, O.G., Georgsson, L.S., and Arnason, K.: Resistivity structure of the Upper Crust in Iceland. J. Geophys. Res. 90(B12), 10136-10150 (1985).

Guéguen, Y. and Dienes, J.: Transport Properties of Rocks from Statistics and Percolation. Math. Geol. 21 (1), 1-13 (1989).

Jaeger, J.C. and Cook, N.G.W.: Fundamentals of rock mechanics. Science Paperbacks. Chapman and Hall, London, 2nd Edition (1976).

Jaya, M.S., Shapiro, S.A., Kristinsdóttir, L.H., Bruhn, D., Milsch, H., and Spangenberg, E.: Temperature-dependence of seismic properties in geothermal rocks at simulated reservoir conditions. Geothermics (in review).

Katz, A.J. and Thompson, A.H.: Quantitative prediction of permeability in porous rock. Phys. Rev. B 34 (11), 8179-8181 (1986).

Katz, A.J. and Thompson, A.H.: Prediction of Rock Electrical Conductivity From Mercury Injection Measurements. J. Geophys. Res. 92 (B1), 599-607 (1987).

Kirkpatrick, S.: Models of disordered materials, in: Balian, R., Maynard, R., Toulouse, G. (Eds.), Ill-Condensed Matter. North-Holland, Amsterdam, 323-403 (1979).

Kristinsdóttir, L.H., Flovenz, O.G., Arnason, K., Bruhn, D., Milsch, H., Spangenberg, E., and Kulenkampff, J.: Laboratory measurements of conductivity of rock samples from Icelandic high temperature geothermal fields as a function of temperature at in-situ conditions. Geothermics (in review).

Kristmannsdóttir, H.: Alteration of basaltic rocks by hydrothermal activity at 100-300°C. In: Developments in Sedimentology, 27 (eds. Mortland, M., and Farmer, V.), pp. 359-367. Elsevier, Amsterdam (1979).

Kühn, M., Frosch, G., Kölling, M., Kellner, T., Althaus, E., and Schulz, H. D.: Experimentelle Untersuchungen zur Barytübersättigung einer Thermalsole, Grundwasser 3, 111–117 (1997).

Kulenkampff, J., Spangenberg, E., Flovenz, O.G., Raab, S., and Huenges, E.: Petrophysical Parameters of Rocks Saturated with Liquid Water at High Temperature Geothermal Reservoir Conditions. In: Proceedings World Geothermal Congress. Antalya, Turkey (2005).

Legarth, B., Huenges, E., and Zimmermann, G.: Hydraulic fracturing in a sedimentary geothermal reservoir: Results and implications. Int. J. Rock Mech. Min. Sci. 42, 1028–1041 (2005).

Martys, N. and Garboczi, E.J.: Length scales relating the fluid permeability and electrical conductivity in random two-dimensional model porous media. Phys. Rev. B 46 (10), 6080-6090 (1992).

Milsch, H., Spangenberg, E., Kulenkampff, J., and Meyhöfer, S.: A new apparatus for long-term petrophysical investigations on geothermal reservoir rocks at simulated in-situ conditions. Transp. Porous Med. 74, 73-85, doi 10.1007/s11242-007-9186-4 (2008a).

Milsch, H., Blöcher, G., and Engelmann, S.: The relationship between hydraulic and electrical transport properties in sandstones: An experimental evaluation of several scaling models. Earth Planet. Sci. Lett. 275, 355-363, doi 10.1016/j.epsl.2008.08.031 (2008b).

Milsch, H., Seibt, A., and Spangenberg, E.: Long-term Petrophysical Investigations on Geothermal Reservoir Rocks at Simulated In Situ Conditions. Transp. Porous Med. 77, 59-78, doi 10.1007/s11242-008-9261-5 (2009).

Milsch, H., Kristinsdóttir, L.H., Spangenberg, E., Bruhn, D., and Flovenz, O.G.: Effect of the water steam phase transition in porous rocks on their electrical conductivity. Geothermics (in review).

Moeck, I., Schandelmeier, H., and Holl, H.-G.: The stress regime in a Rotliegend reservoir of the Northeast German Basin. Int. J. Earth Sci., doi 10.1007/s00531-008-0316-1 (2008).

Omar, A. E.: Effect of brine composition and clay content on the permeability damage of sandstone cores. J. Petroleum Sci. Eng. 4, 245-256 (1990).

Paterson, M.S.: The equivalent channel model for permeability and resistivity in fluid saturated rocks – A reappraisal. Mech. Mater. 2 (4), 345-352 (1983).

Piwinskii, A.J. and Weed, H.C.: A study of rock-solution interaction and its effect on Archie's Law. IEEE Trans. Geosci. Electr. GE-14 (4), 221-223 (1976).

Revil, A., Cathles III, L. M., Losh, S., and Nunn, J. A.: Electrical conductivity in shaly sands with geophysical applications. J. Geophys. Res. 103 (B10), 23925-23936 (1998).

Rink, M. and Schopper, J.R.: Pore structure and physical properties in porous sedimentary rocks. Pure Applied Geophysics 114, 273-284 (1976).

Roberts, J.J., Duba, A.G., Bonner, B.P., and Kasameyer, P.W.: The effects of capillarity on electrical resistivity during boiling in metashale from scientific corehole SB-15-D, The Geysers, California, USA. Geothermics 30, 235-254 (2001).

Ruffet, C., Darot, M., and Guéguen, Y.: Surface conductivity in rocks: A review. Surveys in Geophys. 16, 83-105 (1995).

Scheidegger, A. E.: The physics of flow through porous media. Univ. of Toronto Press, Toronto (1974).

Schepers, A. and Milsch, H.: Effects of fluid-rock interactions in arkosic sandstones: Long-term direct monitoring of changes in permeability, electrical conductivity, and pore fluid chemistry. Geophys. Res. Abstracts 11, EGU2009-5767 (2009).

Seibt, A.: Welche Faktoren können die Eisen(II)-Oxidation in Formationswässern beeinflussen? In: Huenges, E. (ed.) Geothermische Energieentwicklung–geologische und energietechnische Ansatzpunkte. Scientific Technical Report, STR00/23, GeoForschungsZentrum Potsdam, Potsdam, Germany (2000).

Shante, V.K.S.: Hopping conduction in quasi-one-dimensional disordered compounds. Phys. Rev. B 16 (6), 2597-2612 (1977).

Tenthorey, E., Scholz, C. H., Aharonov, E., and Léger, A.: Precipitation sealing and diagenesis: 1. Experimental results. J. Geophys. Res. 103 (B10), 23951-23967 (1998).

Thomas, E.C.: Determination of Qv from membrane potential measurements on shaly sands. Transactions of the American Institute of Mining, Metallurgical, and Petroleum Engineers 261, 1087-1096 (1976).

Ucok, H., Ershaghi, I., and Olhoeft, G.R.: Electrical Resistivity of Geothermal Brines. Journal of Petroleum Technology, pp. 717-727 (1980).

Van Siclen, C.D.: Equivalent channel network model for permeability and electrical conductivity of fracture networks. J. Geophys. Res. 107 (B6), 2106, doi:10.1029/2000JB000057 (2002).

Walsh, J.B. and Brace, W.F.: The Effect of Pressure on Porosity and the Transport Properties of Rock. J. Geophys. Res. 89 (B11), 9425-9431 (1984).

Weast, R.C. (Ed.): CRC Handbook of Chemistry and Physics, 64th Edition. CRC Press, Inc., Boca Raton, FL, USA (1984).

Wyllie, M.R.J. and Rose, W.D.: Some theoretical considerations related to the quantitative evaluation of the physical characteristics of reservoir rock from electrical log data. Trans. Am. Inst. Mech. Eng. 189, 105-118 (1950).

Zimmermann, G., Reinicke, A., Brandt, W., Blöcher, G., Milsch, H., Holl, H.-G., Moeck, I., Schulte, T., Saadat, A., and Huenges, E.: Results of stimulation treatments at the geothermal research wells in Groß Schönebeck/Germany. In: Proceedings 33rd Stanford Workshop on Geothermal Reservoir Engineering. Stanford, USA (2008).